Preformed anodes for high-voltage lithium-ion battery performance: fluorinated electrolytes, crosstalk, and the origins of impedance rise

Adam Tornheim,[a] Ritu Sahore, Meinan He,[a] Jason R. Croy,[a] Zhengcheng Zhang[a,*]

[a] Chemical Sciences and Engineering Division

Argonne National Laboratory

9700 S. Cass Ave., Lemont, IL 60439 USA

Email: zzhang@anl.gov

Abstract

Preformation of graphite electrodes, in a highly fluorinated electrolyte, show exemplary performance when incorporated into $LiNi_{0.5}Mn_{0.3}Co_{0.2}O_2$//graphite cells (NMC//Gr) containing a traditional organic electrolyte. NMC//Gr cells, using preformed graphite electrodes, showed enhanced capacity and power retention as well as improved coulombic efficiencies. The increased performance was only observed with the use of specific electrolytes during the preforming step, where graphite electrodes, when preformed with the baseline organic carbonate electrolyte, did not show the same benefits. The identity of the preforming electrolyte was also observed to influence electrode crosstalk, where compounds generated at one electrode can affect the opposite electrode. The work herein presents both physical and electrochemical evidence of electrode crosstalk and

reveals the beneficial effect of the preforming procedure in limiting the associated degradation mechanisms thereof. The insights gained may lead to new methodologies for the design of electrochemically robust interfaces that can enabling high-voltage, lithium-ion batteries.

Introduction

Layered oxide compounds of the form $LiMO_2$ (M=Co, Ni, Mn, etc.) are commonly used as lithium-ion battery cathodes in the transportation sector due to their intrinsically high volumetric energy densities.[1-2] For these applications, where long cycle life and capacity retention are typically required, the charging voltage of $LiMO_2$ materials must be limited in order to mitigate instabilities of the cathode/electrolyte interface that lead to performance loss.[3-4] For this reason, charging voltages may be limited to just ~4.2 V vs. Li/Li^+, which only accesses 50-60% of the available capacity of the cathode.[5]

Addressing performance losses associated with high charging voltages has long been an area of significant interest with respect to NMC-based oxides. Performance loss in both capacity and power retention has been correlated with electrolyte oxidation at the cathode/electrolyte interface,[6] oxygen loss from the cathode surface,[6-7] surface reorganization of the cathode,[3] HF generation,[8] and transition metal ion dissolution.[1]

As most of these associations are thought to originate from reactions between the electrolyte and the cathode, multiple strategies have been pursued to form protective layers at the cathode/electrolyte interface. These layers can be formed, either in-situ or ex-situ, on the cathode surface to prevent electronic/chemical contact between the electrolyte and the reactive cathode. Strategies include electrolyte additives to form a cathode electrolyte interphase (CEI) layer,[9-12] atomic layer deposited (ALD) coatings to form a protective barrier on the cathode surface,[13-14] and cathode doping with stabilizing metals to limit surface restructuring of the cathode oxide.[15]

Additionally, development of new, less reactive electrolyte solvents have led to fewer electrolyte oxidation reactions at charged, high-voltage, cathode surfaces.[16-18] This reactivity can be diminished by the incorporation of withdrawing groups into the solvent backbone, which in turn lowers the levels of the highest occupied and lowest unoccupied molecular orbitals (HOMO and LUMO, respectively) of the solvent, thereby increasing the anodic stability.[19] While fluorination tends to increase the anodic stability, the lower LUMO levels lead to an additional thermodynamic driving force for cathodic reactions on the anode surface, as the fluorinated solvents are much more reactive at low potentials vs. Li/Li^+ compared to non-fluorinated counterparts.

Most of the strategies aimed at enhancing high-voltage performance are founded on the hypothesis that the reactions between the bulk electrolyte and the cathode

surface are responsible for the performance degradation. In this work, we show that an electrochemical pretreatment of the graphite anode with a highly fluorinated electrolyte, which modifies the identity and composition of the graphite solid-electrolyte interphase (SEI), can substantially improve both the capacity and power retention (i.e., impedance) of $LiNi_{0.5}Mn_{0.3}Co_{0.2}O_2$//graphite cells, even in the absence of modifications to the cathode surface. The results of this work suggest that component(s) in the electrolyte, originating from reductive decomposition of the electrolyte at the graphite anode, are dominant factor(s) contributing to impedance rise, Mn dissolution, and subsequent capacity loss; highlighting the key role of electrode crosstalk in the degradation of NMC//graphite cells at high voltage.

Experimental

Materials

2032 format coin cells were used for all tests. The cathodes were 90% $LiNi_{0.5}Mn_{0.3}Co_{0.2}O_2$ (Toda), 5% PVDF (Solvay 5130), and 5% conductive carbon (Timcal C45), coated onto a 20 μm Al current collector to a gravimetric loading of 9.12 mg/cm^2. The anodes were 91.8% graphite (Philips A12), 0.17% oxalic acid, 2% conductive carbon, and 6% PVdF binder (Kureha 9300) coated onto a 10 μm Cu current collector to a gravimetric loading of 6.07 mg/cm^2. Both electrodes were dried in a vacuum oven at 60ºC for at least four hours to remove adsorbed water before being transferred into an oxygen- and moisture-free glovebox. Cells were

constructed with a 14 mm diameter cathode, a 15 mm diameter anode, and a 16 mm polyolefin separator (Celgard 2325) with 25 μL of electrolyte. Electrolytes used were 1.2 M $LiPF_6$ in a 3/7 weight ratio of EC/EMC (LiPaste A49, Tomiyama), referred to as "Gen2", and a 1.0 M $LiPF_6$ in a 3/7 weight ratio of trans 4,5-difluoroethylene carbonate, referred to as "DFEC" (Solvay), and bis 2,2,2-trifluoroethyl carbonate, referred to as "HFDEC", synthesized according to ref.[20] This highly fluorinated electrolyte is referred to as "FE-3".

Electrochemistry

In this work, two separate electrochemical protocols were used. The "pretreating" protocol, designed to form the initial SEI on the graphite anode, and the "cycling" protocol, designed to evaluate the performance of the battery. Each of these protocols begin with a one hour rest, a 15 minute tap charge at 1.5 V, followed by a 6 hour rest for adequate electrolyte wetting. The cells are then cycled at a C/10 rate (C=2.3 mA) for 5 cycles between 3.0 and 4.4 V (cell voltage) on a battery cycler (Series 4100, Maccor). At this point, the electrochemical pretreating protocol has completed. In the later text, these preformed anodes will be called F-Gr or G-Gr corresponding to preformation with FE-3 or Gen2 electrolytes, respectively. For the subsequent use of pretreated (preformed) electrodes, the cells are removed from the cycler (in the discharged state), disassembled in a glovebox, and recombined with either pristine or preformed electrodes, a new separator, and 25 μL of fresh

Gen2 electrolyte. The pretreated electrodes were not washed, although the solvent residue was allowed to evaporate before the new cell was assembled.

The normal cycling protocol begins with the pretreating protocol and continues with a combination of 1C cycles, C/10 cycles, and modified Hybrid Pulse Power Characterization (HPPC) tests. HPPC tests are performed every 20 cycles to evaluate impedance changes using 10 second, 2C discharge pulses at 10% depth of discharge steps. The majority of cycling time occurs over 100 C/3 ageing cycles with a 3 hour hold at the top of each charge. This cycling protocol is discussed and demonstrated in more detail in previous publications.[21-22]

X-ray photoelectron spectroscopy

Coin cells were decrimped inside an argon-filled glove box having direct connection to an XPS chamber. Anodes and cathodes were extracted and rinsed separately with dimethyl carbonate, dried, and subsequently transferred into the XPS chamber without exposing to air. XPS analysis was performed with a PHI 5000 VersaProbe II System (Physical Electronics) with a base pressure of ~2×10^{-9} Torr. The spectra were obtained using Al Kα radiation ($h\nu$ = 1486.6 eV) (100 μm, 25 W) and Ar^+ and electron beam sample neutralization in Fixed Analyzer Transmission mode. Peak fitting was performed using a Shirley background correction and the Gaussian-Lorentzian curve synthesis available in CasaXPS software. XPS spectra of the cathodes were aligned to the carbon black component in the C1s spectra at 284.7 eV.

XPS spectra of the anodes were aligned to the LiF component in the F1s spectra at 685.6 eV. Manufacturer-reported relative sensitivity factors (RSF) were used to normalize the C1s, O1s, F1s, P2p spectra for plotting such that the area under a region corresponds to the atomic percent of that element in the sample. This normalization allows direct visual comparison of concentration across samples in the series.

Inductively-couple plasma mass spectroscopy (ICP-MS)

Transition metal content of the anodes was evaluated after cycling using a PerkinElmer NexION 2000 ICP Mass Spectrometer, calibrated with NIST standards (Ultra Scientific, USA). The remainder of the harvested graphite electrodes were scraped off the current collector and transferred to a 700ºC oven (overnight) to burn off carbon and other organic content. The remaining residue was dissolved in an acidic medium (10 mL) for ICP-MS analysis. Transition metal content is reported relative to the original (unignited) mass of the sample, with the mass of the copper subtracted. This procedure is essentially repeated from a previous work.[23]

Results

Baseline performance

The performance of cells containing the Gen2 electrolyte is shown in Figure 1. From Figure 1a, an initial discharge capacity of ~190 mAh/g is observed which decays to 163 mAh/g after the full 119 cycles of the protocol, representing 86% capacity retention. The initial coulombic efficiency (CE) is 86%, and in the final C/3 cycles of each 20 cycle "aging set", increases from approximately 99.6% to 99.75%, Figure 1b. The area-specific impedance (ASI), Figure 1c, as determined by the HPPC cycles, increases monotonically at each voltage with increasing cycling. Choosing 3.7 V as a reference voltage, the ASI values increase from 21 Ω-cm^2 to 35 Ω-cm^2 from HPPC cycles 1-5[23], corresponding to 7 and 99 total cycles on test, respectively. This cell will be referred to as "baseline cell" in the later text.

To rule out any effect of the "pretreating" protocol (including decrimping and cell reassembly) in subsequent comparisons with preformed anodes, the Gen2 was tested with the same "pretreatment" protocol, except both the anode and cathode from the pretreatment were recombined in the new cell, instead of a pristine cathode. For these cells, there was no significant change in discharge capacity or CE, although a slight increase in impedance was observed.

Pretreating electrochemistry

Figure 2 shows the pretreating protocol results from both the Gen2 and the FE-3 electrolytes. The Gen2 pretreatment shows similar capacities to the baseline cell performance, which is to be expected (the protocols are identical through the first 5

C/10 cycles). The FE-3 pretreatment shows the same initial charge capacity, followed by lower discharge capacities, indicative of increased lithium trapping during the SEI formation on the first charge (1st cycle CE ~ 75%).

Figure 3 shows the capacities obtained during the pretreating protocol with the FE-3 electrolyte using previously formed and/or pristine electrodes. Figure 3a shows the formation capacities and CE as a function of cycle number for a cell assembled with pristine electrodes. This cell has a low 1st cycle CE of 77%, which subsequently limits the cell capacity to the 1st discharge capacity. After the 1st cycle, the CE increases to 98% and slowly increases through the remaining three cycles. The 1st cycle charge capacity is high, approximately 220 mAh/g, while subsequent charge and discharge capacities are approximately 160 mAh/g.

If the cells shown in Figure 3a are disassembled after the fifth formation cycle, reassembled with a fresh separator and FE-3 electrolyte, and subjected to the same "pretreating" electrochemical protocol, the resulting charge and discharge capacities are as shown in Figure 3b. In Figure 3b, the first charge is approximately the same as the final discharge in Figure 3a, as expected, and a 1st cycle CE of 96% leads to relatively low capacity losses throughout the formation cycles as the CE quickly rises to 99-99.5% for the remaining four cycles.

When the cathodes from formed cells of Figure 3a are harvested and reassembled in cells with a new graphite anode, separator, and FE-3 electrolyte (Figure 3c), the 1st

charge capacity is approximately the same as the final discharge capacity for the cell shown in Figure 3a. However, a CE of 73% lowers the 1st cycle discharge capacity to approximately 120 mAh/g, with slight capacity losses over the subsequent four cycles.

If the FE-3 formed cells in Figure 3a are disassembled and the anode from that cell is combined with a fresh separator, FE-3 electrolyte, and a pristine cathode, the resultant charge and discharge capacities are as shown in Figure 3d. For these cells, the 1st cycle charge capacity is the same as Figure 3a, as a pristine cathode is used in both situations, while subsequent discharge and charge capacities are ~190-195 mAh/g, and slowly rising with each cycle. The 1st cycle CE is approximately 86%, before rising to slightly over 100% for the remaining four cycles.

Pretreated graphite electrochemistry

Cycling

Figure 4a shows the cycling protocol results with both preformed and pristine graphite when combined with pristine cathodes. Graphite pretreated with the FE-3 electrolyte (F-Gr) and graphite pretreated with the Gen2 electrolyte (G-Gr) both show a high initial CE of 87.5% as well as discharge capacities of ~197 mAh/g. Both F-Gr and G-Gr containing cells maintain this high discharge capacity for a number of cycles before showing any capacity fade, in contrast to the baseline cells with

pristine graphite electrodes, which show capacity fade immediately. The final capacities for the preformed graphite cells are 189 mAh/g and 179 mAh/g for the F-Gr and G-Gr containing cells, respectively. The CEs of both F-Gr and G-Gr containing cells start higher than the baseline, although Figure 4b shows that F-Gr cells approach a higher CE (99.88%) during the final aging cycles compared with the G-Gr containing cells (99.71%), which is lower than that of the baseline (99.75%)

Impedance

The HPPC results for the pretreated graphite cells are shown in Figure 5. Compared to the baseline system, the initial ASI for both the preformed graphite cells is higher, with F-Gr leading to an ASI at ~3.7 V of 36 Ω-cm^2 compared to 29 Ω-cm^2 for G-Gr (Table 1). However, the impedance rise from the first HPPC (cycle 7) to the final HPPC (cycle 99) is dramatically lower for the F-Gr compared to G-Gr (13% vs. 92%). The same trends are seen for the impedance at 4.2 V. In addition, the final ASI is lower for the F-Gr compared to the G-Gr across all stages of charge.

Post-cycling characterization

After the ~120 cycles shown in Figure 4a, the cells were decrimped and electrodes were analyzed with XPS. ICP-MS was used to measure the transition metal content of anodes. The XPS spectra for both the anodes and cathodes are shown in Figures 6. For the cycled anodes that were preformed in FE-3 (F-Gr), there is slightly more fluorine and phosphorus compared to the cycled anodes that were preformed in the Gen2 baseline (G-Gr), but there is more oxygen observed with the G-Gr. The spectra

of the cycled cathodes do not show a substantial dependence on the identity of the preforming electrolyte. However, the low binding energy area of the graphite XPS spectra show significant lithium content for the Gen2 formed graphite, while the F-Gr also shows significant amounts of transition metals (nickel and manganese).

ICP-MS results for the anodes after the full cycling protocol are shown in Figure 7. Transition metal content in the anode is attributed to degradation of the cathode, and Mn content, in particular, has been correlated with capacity fade from additional lithium trapping due to electrolyte decomposition. Figure 7 shows that while there is significantly more nickel and cobalt for the FE-3 preformed graphite, the manganese content is higher with the Gen2 preformed graphite.

Discussion

Understanding the initial cycling and CE

In order to understand the cycling performance of the cells with the preformed graphite electrodes, it is necessary to understand how coulombic inefficiencies and Li trapping can change the cycleable lithium content of the cells.

The reactivity of graphite anodes has been studied extensively, and leads to irreversible capacity loss (ICL) as the lithiated graphite reduces the electrolyte to form the passivating SEI layer. The amount of ICL will depend both on electrolyte identity as well as graphite morphology.[24-26] The low 1st CE associated with the FE-3

electrolyte in Figure 3a is consistent with lithium trapping that arises through SEI formation. As the cathode is delithiated and lithium is intercalated into the anode, the voltage of the anode drops, increasing the Fermi level of the anode above the LUMO of an electrolyte component, which leads to the electrochemical reduction of that component and the loss of a lithium atom to the electrolyte. The charge capacity of a cell is less affected by this phenomenon (as shown in Figure 2), as the lower graphite plateau extends for though the latter half the anode capacity. As long as the SEI-forming reactions do not trap enough lithium to change the voltage plateau of the graphite at the end of charge, the cell potential is determined by cathode state of charge. However, upon discharge, the graphite has fewer intercalated lithium ions than there are vacancies in the cathode, and the discharge is completed when the graphite can no longer supply lithium ions and thus polarizes; referred to as the premature polarization of the graphite anode. Thus, as 1st charge capacities are the same for the two electrolytes, the 1st discharge capacities are very different, depending on Li trapping differences of the two electrolytes.

After the first cycle, the capacity transferred between the electrodes is roughly the amount of capacity left in the graphite anode after the first charge cycle, as the graphite anode has been mostly passivated to electrolyte reduction and the lithium trapping has been arrested. In Figure 1, CEs of ~99% coupled with slight capacity losses per cycle is consistent with additional reduction reactions at anodes that have not been completely passivated.

The results in Figure 3b show, in part, an evaluation of the disassembly protocol. Here, harvested electrodes from the cells shown in Figure 3a are reassembled with fresh FE-3. If there is no change to either electrode, the capacities should resume where they ended in cycle 5 in Figure 3a. However, the lower 1st cycle CE of 96%, compared to 99% for the final cycle for the cells in Figure 3a, indicates some amount of the anode has to be passivated after reassembly. This lower CE could arise through a combination of damage to the SEI, requiring repassivation, or a slight change in alignment of the electrodes,[21] leading to non-passivated (unactivated) graphite surface directly across from the cathode, necessitating a first lithiation and SEI formation (ICL) of a new section of the graphite electrode.

The cells in Figure 3c essentially repeat the lithium trapping process responsible for the low capacity in Figure 3a. For the cells shown in 3c, a pristine anode is combined with a cathode extracted from a formed cell, in which the cathode is not fully lithiated due to the ICL processes described earlier. In this cell, the first charge capacity is governed by the amount of lithium in the cathode, but the first discharge capacity is lower by approximately 0.7 mAh, the same as the side-reaction capacity for the first cycle in Figure 3a. The CE again slowly increases as the capacity decreases slightly over the remaining four cycles, due to the same possible processes discussed for Figure 3a.

The results in Figure 3d can be partially explained by examining the results of the other cells shown in Figures 3a-3c. The cells in 3d were assembled with pristine cathodes and FE-3 formed anodes, which led to the same 1st charge capacity as seen in Figure 3a. However, it can be seen from Figure 3b showing reassembled, preformed cathode and anode electrodes, that the preformed anodes used in the cells in Figure 3d are mostly passivated, as the ICL is only about 0.05 mAh (~4%). For Figure 3d, the 1st cycle CE of 87% would not be explained by lithium trapping, as the same amount of lithium trapping as seen in Figure 3b, with a previously formed anode, would result in a 1st cycle discharge capacity of 2.75 mAh and a CE of ~97%. Thus, the lower CE observed in Figure 3d must arise through a different process.

The low 1st cycle CE shown in Figure 3d could arise through sluggish kinetics at the cathode. $LiMO_2$ cathodes at very low states of charge are known to have slow kinetics, which is indicative of the slow lithium intercalation of a nearly fully lithiated cathode.[27-28] At low enough cycling rates, much of this ICL at the cathode can be recovered, but the rates used in this work are high enough that the current density results in the polarization of the cathode and the lower cutoff voltage in the electrochemical testing protocol is reached. After the first cycle, the CE rises to just above 100%, although this is due to a slow increase in measured capacity. This is hypothesized to arise from a small amount of lithium still present in the anode after the formation protocol.

The explanation of the cycling behavior from Figure 3d is also applicable to the Gen2 preformed graphite cells showing CE greater than 100 for the initial cycles (Figure 4d). One observation contrasting the preformed graphites with pristine graphite, when cycled with the baseline electrolyte, is the initial excellent capacity retention with the F-Gr and G-Gr cells, Figure 4a. The reason for this becomes clear after the lithium inventory for each electrode is examined. NMC-cathodes, like NMC-532 used herein, have an irreversible capacity loss (ICL) on the first cycle of ~25 mAh/g, which has been attributed to kinetic effects in the mostly discharged cathode. The anode used in this study has an initial CE of ~90% with the Gen2 electrolyte, which corresponds to a 1st cycle ICL of 30 mAh/g (as measured in terms of cathode capacity for this electrode pair). The difference between these two ICLs is the difference between the initial capacity of the Gen2 electrolyte with pristine electrodes (190 mAh/g) and the preformed cells (~197 mAh/g), as well as the respective CEs, even though the first charge capacities are the same, at ~220 mAh/g. However, this 5 mAh/g difference between the preformed cells and the baseline cells is indicative of a different state of the lithium inventory. For the baseline cells, the Li trapping at the anode during the 1st charge limits the amount of cycleable lithium in the system, such that the first discharge step ends when the anode is fully delithiated (190 mAh/g in the cathode), even though the cathode can accommodate 5 mAh/g more lithium. With the preformed graphite, the 1st cycle ICL from Li trapping is minimized (because the graphite already has a functional SEI), and so the 1st discharge cycle terminates because the cathode cannot accept more lithium (195 mAh/g). At this time, the anode still has cycleable lithium, but the cathode has

polarized in response to the applied discharge current and the discharge step ends (cell voltage < 3.0 V). As it has already been established that the capacity loss in these cells is due to reduction reactions at the anode, the reservoir of excess cycleable lithium in the preformed anodes has to be depleted before the discharge step ends when the anode is fully delithiated, at which point capacity loss from Li trapping could be observed. In this way, there is a "cushion" of excess lithium that allows no capacity loss due to "electrode slippage"[29] until the excess lithium has been consumed. This cushion effect is very evident in the G-Gr cells at cycle ~30, Figure 3a, after which the capacity starts to fade at roughly the same rate as the baseline cells. For the F-Gr cells, the superior capacity retention extends significantly into the cycling protocol, such that at the end of the 119 cycles, the capacity has only dropped ~4.5%, compared to the 13% of the baseline electrolyte. This reveals that the SEI formed on graphite with the FE-3 electrolyte is substantially more robust than the SEI formed by the baseline Gen2, as evidenced by the number of cycles required to consume the excess lithium in the anode through electrolyte reduction.

Impedance rise

Comparing the ASIs for the G-Gr/pristine cathode cell (Table 1) and the baseline cell (Figure 1) shows only small differences, which may be due to either the additional cycles in the pretreatment (for the graphite only) or any damage to the cells occurring during the opening and reassembly process. Comparing either the

baseline or the G-Gr containing cells to the F-Gr containing cells (pristine cathodes) shows that the F-Gr containing cells have significantly lower impedance rise with increasing HPPC cycle number (Table 1).

The trends in the ASI of the cells containing pretreated graphite anodes compared with the baseline system are most surprising. Previous research has indicated that the impedance rise with high voltage $LiMO_2$ cathodes occurs predominantly at the cathode, while the anode impedance remains low, and the capacity loss is due to continuous reduction reactions at the anode which decrease the amount of cycleable lithium in the system (lithium trapping).[30] Unlike the $LiMO_2$ cathodes, the potential of a graphite anode is not significantly affected by the full cell upper cutoff voltage, so to a first approximation there should not be additional electrolyte reactions at the anode at high states of charge. However, at high voltage, the transition metal ions in the cathode will dissolve into the electrolyte and migrate across the cell to the anode, where they can catalyze additional reduction reactions. As mentioned previously, capacity fade was thought to originate from reduction reactions at the anode, and electrode crosstalk (components that are generated at one electrode and react at the opposite electrode) has been shown to affect the rate of these reduction reactions.[31] One common example is Mn ion dissolution, which originates at the cathode but catalyzes reduction reactions at the anode to lead to additional capacity fade.[4, 32] While it is reasonable to expect that altering the identity of the SEI would change the reduction rate of the electrolyte on the anode (e.g., Li loss, Figure 4), the impedance rise over the course of the cycling protocol

would not be expected to depend on anode pretreatment, as the dominant factor for impedance rise is typically rationalized in terms of reactions between the electrolyte and the cathode.

The results in Figure 5 show the dependence of cell ASI on identity of the pretreating electrolyte. As the impedance data of Figure 5 shows a strong dependence on pretreating electrolyte, it can be concluded that the Gen2-formed graphite anode must have a negative effect on the cathode impedance rise through crosstalk, and the FE-3 pretreatment of the graphite must therefore limit the effect. The simplest rationale for these HPPC results is that a soluble component from Gen2 reduction on graphite leads to the impedance rise on the cathode, and the superior passivation of the graphite by the FE-3 electrolyte limits further Gen2 reduction, and therefore prevents the generation of this deleterious component. This is not the first time that anode-to-cathode crosstalk has been reported,[33] however, the results in this manuscript infer specific negative effects associated with the presence of anode-cathode crosstalk as discussed below.

One important takeaway in looking at the superior performance enabled by the F-Gr over the G-Gr is that the identity of the pretreating electrolyte is crucial in realizing impedance and capacity retention benefits of a stabilized graphite SEI. While any pretreatment of the graphite will form an SEI and limit the 1st charge ICL (leading to a temporary capacity retention increase), only specific pretreating electrolytes will stabilize the SEI of the graphite and lead to better capacity retention and lower

impedance rise, in effect, stabilizing both cathode/electrolyte and anode electrolyte interfaces over long-term cycling.

Source of the effect

Proof of robust SEI with FE-3 electrolyte

One of the characteristics of both cathodes and anodes after formation with the FE-3 electrolyte is a substantial amount of electrolyte decomposition products at the surface that could be detected through XPS (Figure 8e), obscuring any of the underlying transition metal peaks (Figure 8e), carbon black peak at 284.7 eV (Figure 8a), and TM-oxide peak at 529.6 eV (Figure 8b) of the bulk cathode material (blue curve). At first glance, the presence of these surface species could be attributed to electrolyte decomposition reactions at both electrodes. However, after the 5 formation cycles using F-Gr as an anode and a pristine cathode using the FE-3 electrolyte (as in Figure 3d), we observe significantly less amount of surface species on the cathode (red curve). This result leads to two main conclusions about the SEI formation with the FE-3 electrolyte:

1. The majority of surface species on the cathode, after formation with the pristine anode, are not due to electrolyte decomposition reaction at the cathode, but rather, to the formation of soluble reduction products at the anode that then migrate to the cathode and adhere.

2. The FE-3 reduction on the graphite during the first 5 cycles forms an extremely robust SEI that limits further electrolyte reduction (with fresh FE-3 electrolyte), and thus minimizes the presence of surface species on the cathode.

This was confirmed further by using a preformed cathode from a FE-3 pretreatment cell and combining with a pristine graphite anode and fresh FE-3 electrolyte, and cycled according to the pretreatment protocol (green curve). This cathode, therefore, had then been subjected to two SEI formations with the FE-3 electrolyte, which led to an even larger amount of surface species presence (green curve), as evident by the largest suppression of carbon black/TM-oxide peak in this case. A huge lithium peak is also observed in this case indicating that the cross-talk species are likely lithium-containing. The observations in Figure 8 are important in that they demonstrate evidence of anode-cathode crosstalk species.

Further evidence of the relative graphite passivation strength of the FE-3 electrolyte was demonstrated through an experiment in which cathodes and anodes were formed (5, C/10 cycles) in the Gen2 electrolyte, disassembled, and cycled again in the FE-3 electrolyte. Figure 9 shows the charge and discharge capacities of each of these cells for the first cycle after reassembly. After reassembly with the FE-3 electrolyte, these cells showed an initial charge capacity of ~190 mAh/g followed by an initial discharge capacity of ~150 mAh/g, which is comparable to the 1st cycle discharge capacity of pristine electrodes cycled with the FE-3 electrolyte. This

indicates that the Gen2 electrolyte can passivate the graphite electrode with respect to further *Gen2 reduction*, but *not* with respect to *FE-3 reduction*, shown by the large capacity loss for the 'Gen2 formed, FE-3 cycled' cells in Figure 9. Interestingly, the 1st cycle discharge capacities for the pristine electrodes with FE-3 electrolyte and the Gen2-formed electrodes with the FE-3 electrolyte are the same, indicating that *the same number of reduction (Li-trapping) reactions are required to passivate the graphite to FE-3 reduction*. Though speculation at this point, one possible explanation is that the while the Gen2 electrolyte reacts on the edge planes,[24] the FE-3 electrolyte reacts on both edge and basal planes, providing more protection to electrolyte reduction through additional passivated surfaces.

Additional corroboration of the passivation properties of the FE-3 electrolyte can be observed in the post-cycling characterization. At first glance, the XPS results (top 10 nm of the SEI) indicate significant amounts of both Ni and Mn in the SEI of the FE-3 preformed graphite, while the Gen2 preformed graphite does not show these peaks. However, the ICP results indicate significantly more Mn in the Gen2 preformed graphite. These seemingly contradictory results can be rationalized in the following way. The SEI on the graphite is likely significantly thicker than the penetration depth of the XPS. While the top surface of the SEI with the FE-3 preformed graphite is enriched with Mn (compared with the Gen2-preformed graphite), the bulk of the SEI, as measured by the ICP-MS, shows substantially less. This indicates that Mn that has been dissolved from that cathode and travels to the anode is less able to penetrate the outer layer of the FE-3-formed SEI, and therefore the concentration at

the graphite surface is lower. However, recent work by Gilbert et al. found that while Ni, Co, and Mn all dissolve into the electrolyte from the cathode, Mn had the strongest correlation with capacity loss (Li trapping).[4] As there is also significantly more Mn in the Gen2-preformed graphite, this would contribute to the additional capacity fade as compared to the FE-3-preformed graphite. Previous works have shown that the mechanisms associated with Mn dissolution and migration depend on the complexing environment.[32, 34] As the nature of the SEI is changed by the FE-3 electrolyte, fewer, or perhaps more benign, soluble reduction products will be available to participate in Mn complexation and dissolution processes.

Similar to the rationale for the ASI dependence on preforming electrolyte identity, in that a soluble reduction component from the Gen2-formed anode is likely contributing to the impedance rise, TM dissolution (which clearly originates from the cathode) is also found to depend strongly on the nature of the SEI formed on the graphite. This suggests that an important component/ligand for Mn dissolution originates from continual Gen2 reduction at the anode. If this process is slowed with proper passivation, Mn dissolution is hindered.

Conclusions

In this work, a series of preforming experiments, on both cathodes and anodes, was preformed to determine the influence of preforming electrolyte identity on SEI

stability. The two electrolytes used for the preforming treatments were as baseline, EC/EMC containing electrolyte and a highly fluorinated electrolyte composed of DFEC and HFDEC solvents. Our results indicate the following conclusions:

1. The fluorinated electrolyte formed a highly stable, passivating layer on graphite anodes that increased the capacity retention when used with a pristine cathode and the baseline electrolyte, due to fewer Li trapping reactions at the anode.
2. The cells using the FE-3-formed graphite showed significantly lower impedance rise. Impedance rise is conventionally attributed to the cathode-electrolyte interface and the observed improvement points to crosstalk as a major contributor to impedance rise, rather than just reactions with the baseline electrolyte at the cathode interface.
3. Post-test characterization revealed fewer Mn ions in the SEI of the graphite formed with the fluorinated electrolyte. In addition, those Mn ions were found in higher concentration at the surface of the SEI compared to the bulk. Combined with the electrochemical data, this observation directly implicates soluble reduction species from the baseline SEI as possible complexing agents for Mn dissolution, as well as the resistance of the FE-3 SEI to Mn transport.

Acknowledgements

The authors would like to thank J. Gilbert for his assistance with the baseline electrolyte performance. We also thank D. Graczyk and Y. Tsai for ICP-MS analysis of

our samples, which was conducted at Argonne's Analytical Chemistry Laboratory. The electrodes used in this article were fabricated at Argonne's Cell Analysis, Modeling and Prototyping (CAMP) Facility. Support from the Vehicle Technologies Office (VTO), Hybrid Electric Systems Program, David Howell (Manager), Battery R&D, Peter Faguy (Technology Manager), at the U.S. Department of Energy, Office of Energy Efficiency and Renewable Energy, is gratefully acknowledged. The CAMP Facility is fully supported by the VTO within the core funding of the Applied Battery Research (ABR) for Transportation Program. The submitted manuscript has been created by UChicago Argonne, LLC, Operator of Argonne National Laboratory ("Argonne"). Argonne, a U.S. Department of Energy Office of Science laboratory, is operated under Contract No. DE-AC02- 06CH11357.

References

1. Zheng, H.; Sun, Q.; Liu, G.; Song, X.; Battaglia, V. S., Correlation between dissolution behavior and electrochemical cycling performance for LiNi1/3Co1/3Mn1/3O2-based cells. *J. Power Sources* **2012,** *207*, 134-140.

2. Croy, J. R.; Abouimrane, A.; Zhang, Z., Next-generation lithium-ion batteries: The promise of near-term advancements. *MRS Bull.* **2014,** *39* (5), 407-415.

3. Jung, S.-K.; Gwon, H.; Hong, J.; Park, K.-Y.; Seo, D.-H.; Kim, H.; Hyun, J.; Yang, W.; Kang, K., Understanding the Degradation Mechanisms of LiNi0.5Co0.2Mn0.3O2 Cathode Material in Lithium Ion Batteries. *Advanced Energy Materials* **2014,** *4* (1), n/a-n/a.

4. Gilbert, J. A.; Shkrob, I. A.; Abraham, D. P., Transition Metal Dissolution, Ion Migration, Electrocatalytic Reduction and Capacity Loss in Lithium-Ion Full Cells. *J. Electrochem. Soc.* **2017,** *164* (2), A389-A399.

5. Nitta, N.; Wu, F.; Lee, J. T.; Yushin, G., Li-ion battery materials: present and future. *Mater. Today* **2015,** *18* (5), 252-264.

6. Jung, R.; Metzger, M.; Maglia, F.; Stinner, C.; Gasteiger, H. A., Oxygen Release and Its Effect on the Cycling Stability of LiNixMnyCozO2 (NMC) Cathode Materials for Li-Ion Batteries. *J. Electrochem. Soc.* **2017,** *164* (7), A1361-A1377.

7. Jung, R.; Metzger, M.; Maglia, F.; Stinner, C.; Gasteiger, H. A., Chemical versus Electrochemical Electrolyte Oxidation on NMC111, NMC622, NMC811, LNMO, and Conductive Carbon. *The Journal of Physical Chemistry Letters* **2017**, 4820-4825.

8. Shkrob, I. A.; Abraham, D. P., Electrocatalysis Paradigm for Protection of Cathode Materials in High-Voltage Lithium-Ion Batteries. *The Journal of Physical Chemistry C* **2016,** *120* (28), 15119-15128.

9. Park, Y.; Shin, S. H.; Hwang, H.; Lee, S. M.; Kim, S. P.; Choi, H. C.; Jung, Y. M., Investigation of solid electrolyte interface (SEI) film on LiCoO2 cathode in fluoroethylene carbonate (FEC)-containing electrolyte by 2D correlation X-ray photoelectron spectroscopy (XPS). *J. Mol. Struct.* **2014,** *1069*, 157-163.

10. Xu, M.; Tsiouvaras, N.; Garsuch, A.; Gasteiger, H. A.; Lucht, B. L., Generation of Cathode Passivation Films via Oxidation of Lithium Bis(oxalato) Borate on High Voltage Spinel (LiNi0.5Mn1.5O4). *The Journal of Physical Chemistry C* **2014,** *118* (14), 7363-7368.

11. Yang, L.; Ravdel, B.; Lucht, B. L., Electrolyte Reactions with the Surface of High Voltage LiNi0.5Mn1.5O4 Cathodes for Lithium-Ion Batteries. *Electrochem. Solid-State Lett.* **2010,** *13* (8), A95-A97.

12. Zhu, Y.; Li, Y.; Bettge, M.; Abraham, D. P., Positive Electrode Passivation by LiDFOB Electrolyte Additive in High-Capacity Lithium-Ion Cells. *J. Electrochem. Soc.* **2012,** *159* (12), A2109-A2117.

13. Dahlberg, K.; Mohanty, D.; Lee, M.; Anderson, E.; Mahajan, V.; Stanley, J.; King, D. M.; Wood, D. L.; Albano, F. In *Layered-to-Spinel Phase Transformations Inhibited By ALD Coatings on NMC Cathodes to Mitigate Voltage Fade in Lithium-Ion Cells*, Meeting Abstracts, The Electrochemical Society: 2015; pp 450-450.

14. Li, X.; Liu, J.; Banis, M. N.; Lushington, A.; Li, R.; Cai, M.; Sun, X., Atomic layer deposition of solid-state electrolyte coated cathode materials with superior high-voltage cycling behavior for lithium ion battery application. *Energy & Environmental Science* **2014,** *7* (2), 768-778.

15. Kam, K. C.; Mehta, A.; Heron, J. T.; Doeff, M. M., Electrochemical and Physical Properties of Ti-Substituted Layered Nickel Manganese Cobalt Oxide (NMC) Cathode Materials. *J. Electrochem. Soc.* **2012,** *159* (8), A1383-A1392.

16. He, M.; Hu, L.; Xue, Z.; Su, C. C.; Redfern, P.; Curtiss, L. A.; Polzin, B.; von Cresce, A.; Xu, K.; Zhang, Z., Fluorinated Electrolytes for 5-V Li-Ion Chemistry: Probing Voltage Stability of Electrolytes with Electrochemical Floating Test. *J. Electrochem. Soc.* **2015,** *162* (9), A1725-A1729.

17. Hu, L.; Zhang, Z.; Amine, K., Fluorinated electrolytes for Li-ion battery: An FEC-based electrolyte for high voltage LiNi 0.5 Mn 1.5 O 4/graphite couple. *Electrochem. Commun.* **2013,** *35*, 76-79.

18. Su, C.-C.; He, M.; Tornheim, A.; Cao, J.; Redfern, P.; Curtiss, L. A.; Shkrob, I. A.; Zhang, Z., Oxidatively Stable Fluorinated Sulfones Electrolytes for High Voltage High Energy Li-Ion Batteries. *Meeting Abstracts* **2018,** *MA2018-01* (3), 570.

19. Zhang, Z.; Hu, L.; Wu, H.; Weng, W.; Koh, M.; Redfern, P. C.; Curtiss, L. A.; Amine, K., Fluorinated electrolytes for 5 V lithium-ion battery chemistry. *Energy & Environmental Science* **2013,** *6* (6), 1806-1810.

20. He, M.; Su, C. C.; Feng, Z.; Zeng, L.; Wu, T.; Bedzyk, M. J.; Fenter, P.; Wang, Y.; Zhang, Z., High Voltage LiNi0.5Mn0.3Co0.2O2/Graphite Cell Cycled at 4.6 V with a FEC/HFDEC‐Based Electrolyte. *Advanced Energy Materials* **2017,** *7* (15), 1700109.

21. Long, B. R.; Rinaldo, S. G.; Gallagher, K. G.; Dees, D. W.; Trask, S. E.; Polzin, B. J.; Jansen, A. N.; Abraham, D. P.; Bloom, I.; Bareño, J.; Croy, J. R., Enabling High-Energy, High-Voltage Lithium-Ion Cells: Standardization of Coin-Cell Assembly, Electrochemical Testing, and Evaluation of Full Cells. *J. Electrochem. Soc.* **2016,** *163* (14), A2999-A3009.

22. Tornheim, A.; Peebles, C.; Gilbert, J. A.; Sahore, R.; Garcia, J. C.; Bareño, J.; Iddir, H.; Liao, C.; Abraham, D. P., Evaluating electrolyte additives for lithium-ion cells: A new Figure of Merit approach. *J. Power Sources* **2017,** *365*, 201-209.

23. Peebles, C.; Sahore, R.; Gilbert, J. A.; Garcia, J. C.; Tornheim, A.; Bareño, J.; Iddir, H.; Liao, C.; Abraham, D. P., Tris (trimethylsilyl) Phosphite (TMSPi) and Triethyl Phosphite (TEPi) as Electrolyte Additives for Lithium Ion Batteries:

Mechanistic Insights into Differences during LiNi0. 5Mn0. 3Co0. 2O2-Graphite Full Cell Cycling. *J. Electrochem. Soc.* **2017,** *164* (7), A1579-A1586.

24. Zaghib, K.; Nadeau, G.; Kinoshita, K., Effect of Graphite Particle Size on Irreversible Capacity Loss. *J. Electrochem. Soc.* **2000,** *147* (6), 2110-2115.

25. Xia, J.; Sinha, N.; Chen, L.; Dahn, J., A comparative study of a family of sulfate electrolyte additives. *J. Electrochem. Soc.* **2014,** *161* (3), A264-A274.

26. Xia, J.; Nie, M.; Burns, J. C.; Xiao, A.; Lamanna, W. M.; Dahn, J. R., Fluorinated electrolyte for 4.5 V Li(Ni0.4Mn0.4Co0.2)O2/graphite Li-ion cells. *J. Power Sources* **2016,** *307*, 340-350.

27. Kang, S.-H.; Yoon, W.-S.; Nam, K.-W.; Yang, X.-Q.; Abraham, D. P., Investigating the first-cycle irreversibility of lithium metal oxide cathodes for Li batteries. *Journal of Materials Science* **2008,** *43* (14), 4701-4706.

28. Kasnatscheew, J.; Evertz, M.; Streipert, B.; Wagner, R.; Klöpsch, R.; Vortmann, B.; Hahn, H.; Nowak, S.; Amereller, M.; Gentschev, A.-C., The truth about the 1st cycle Coulombic efficiency of LiNi 1/3 Co 1/3 Mn 1/3 O 2 (NCM) cathodes. *PCCP* **2016,** *18* (5), 3956-3965.

29. Smith, A. J.; Burns, J. C.; Xiong, D.; Dahn, J. R., Interpreting High Precision Coulometry Results on Li-ion Cells. *J. Electrochem. Soc.* **2011,** *158* (10), A1136-A1142.

30. Gilbert, J. A.; Bareño, J.; Spila, T.; Trask, S. E.; Miller, D. J.; Polzin, B. J.; Jansen, A. N.; Abraham, D. P., Cycling Behavior of NCM523/Graphite Lithium-Ion Cells in the 3–4.4 V Range: Diagnostic Studies of Full Cells and Harvested Electrodes. *J. Electrochem. Soc.* **2017,** *164* (1), A6054-A6065.

31. Xiong, D. J.; Ellis, L. D.; Petibon, R.; Hynes, T.; Liu, Q. Q.; Dahn, J. R., Studies of Gas Generation, Gas Consumption and Impedance Growth in Li-Ion Cells with Carbonate or Fluorinated Electrolytes Using the Pouch Bag Method. *J. Electrochem. Soc.* **2017,** *164* (2), A340-A347.

32. Shkrob, I. A.; Kropf, A. J.; Marin, T. W.; Li, Y.; Poluektov, O. G.; Niklas, J.; Abraham, D. P., Manganese in Graphite Anode and Capacity Fade in Li Ion Batteries. *The Journal of Physical Chemistry C* **2014,** *118* (42), 24335-24348.

33. Vadivel, N. R.; Ha, S.; He, M.; Dees, D.; Trask, S.; Polzin, B.; Gallagher, K. G., On Leakage Current Measured at High Cell Voltages in Lithium-Ion Batteries. *J. Electrochem. Soc.* **2017,** *164* (2), A508-A517.

34. Aoshima, T.; Okahara, K.; Kiyohara, C.; Shizuka, K., Mechanisms of manganese spinels dissolution and capacity fade at high temperature. *J. Power Sources* **2001,** *97-98*, 377-380.

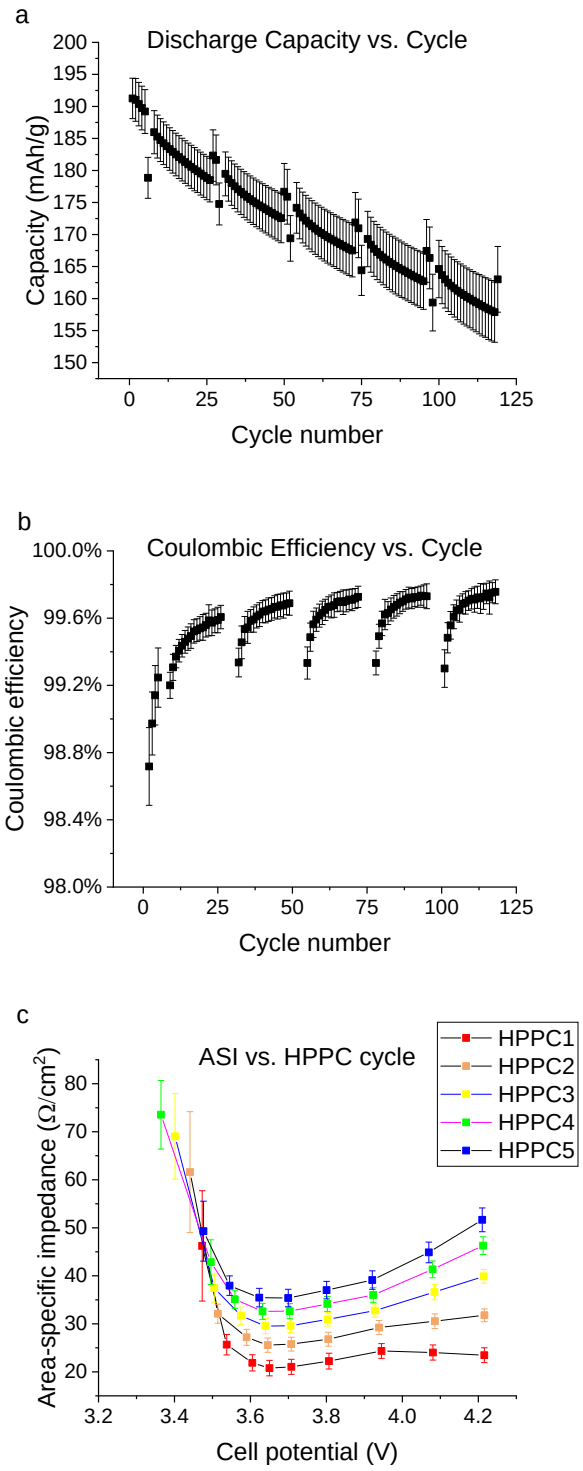

Figure 1. Discharge capacity vs. cycle number (a), CE vs. cycle number (b), and ASI vs. voltage (c) for the baseline system. Each point represents the average of at least 3 cells with the error bars indicating the standard deviation.

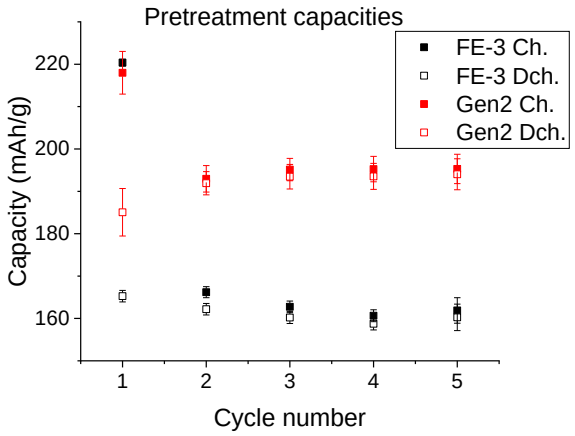

Figure 2. Charge and discharge capacities for FE-3 and Gen2 electrolytes for the pretreating protocol. Each data point is the average of 3 cells with the standard deviation indicated by the error bars.

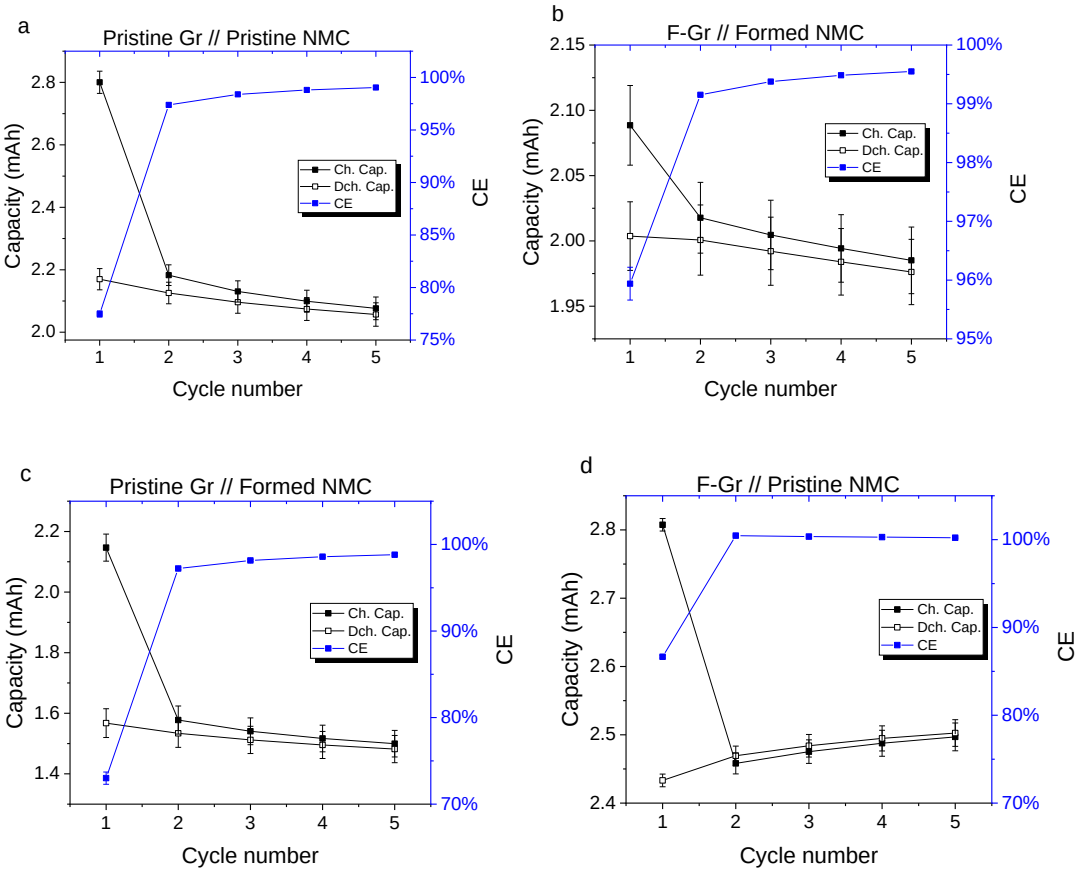

Figure 3. Charge and discharge capacities and CE for four preforming conditions. (a) pristine graphite and NMC532 in FE-3 electrolyte. (b) The electrodes from (a) after decrimping and reassembly with fresh FE-3 electrolyte. (c) The cathode from (a) combined with a pristine anode and fresh FE-3 electrolyte. (d) The anode from (a) combined with a pristine cathode and fresh FE-3 electrolyte. Each data point is the average of 3 cells with the standard deviation indicated by the error bars.

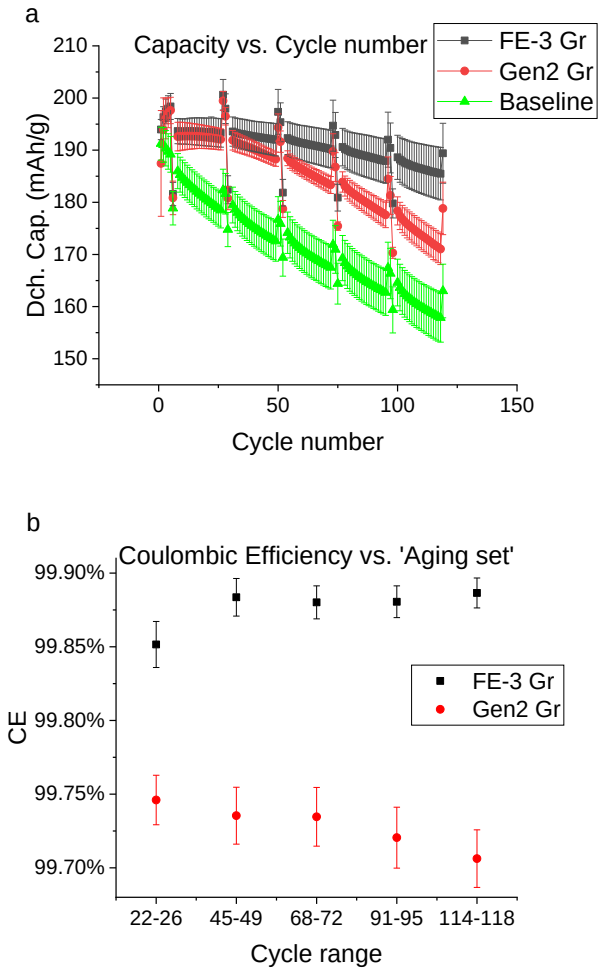

Figure 4. (a) Capacity vs. cycle number for cells containing pristine graphite/F-Gr/G-Gr anodes, pristine cathodes, and Gen2 electrolyte. (b) Average CE for the final 5 C/3 cycles of each "aging set", directly before the C/10 cycles. Each data point is the average of 3 cells with the standard deviation indicated by the error bars.

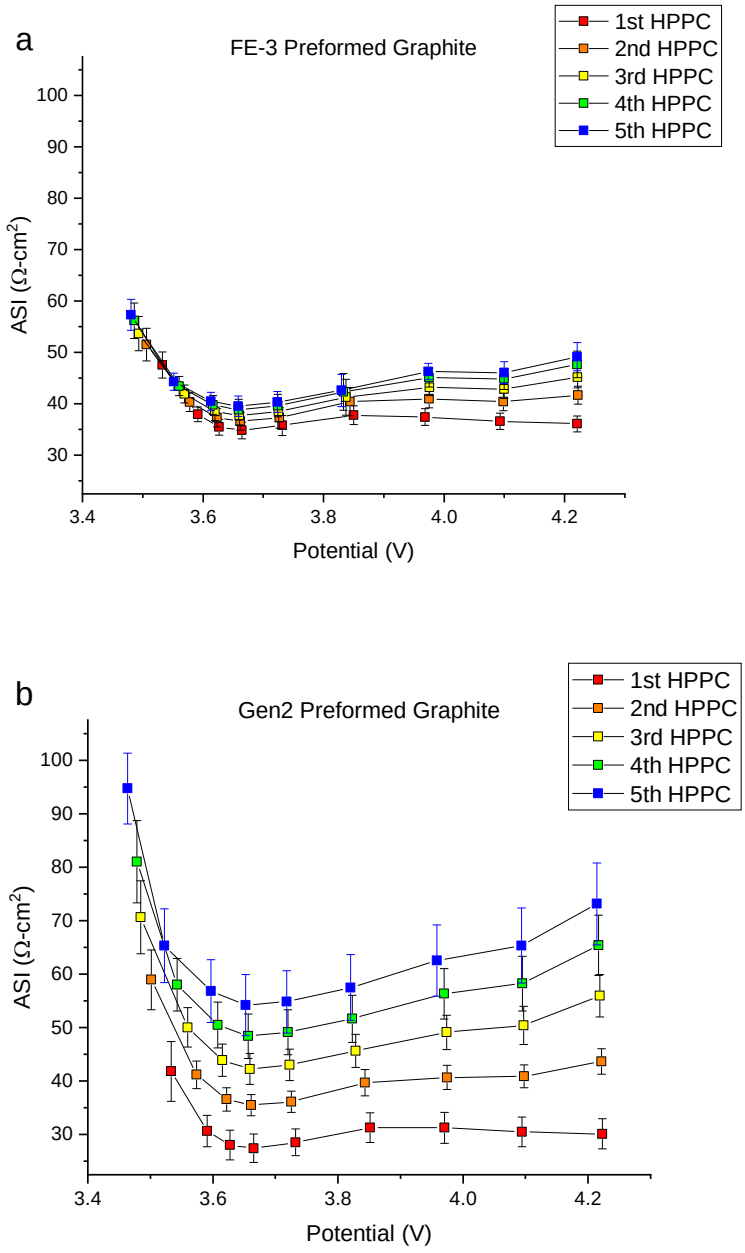

Figure 5. ASI as a function of voltage as evaluated by HPPC tests at cycles 7, 30, 53, 76, and 99 for F-Gr (a) and G-Gr (b) anodes. Each data point is the average of 3 cells with the standard deviation indicated by the error bars.

Table 1. ASI (Ω/cm^2) as determined by the first and last HPPC tests for the cells with preformed graphite anodes

	Cycle 7	Cycle 99	% increase
F-Gr ~4.2V	36	49	36%
G-Gr ~4.2V	30	73	143%
F-Gr ~3.7V	36	40	13%
G-Gr ~3.7V	29	55	92%

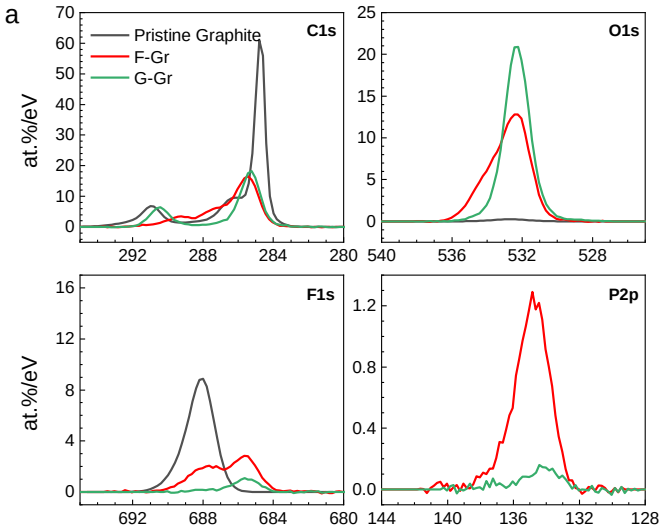
a
Pristine Graphite
F-Gr
G-Gr
C1s
O1s
F1s
P2p
at.%/eV

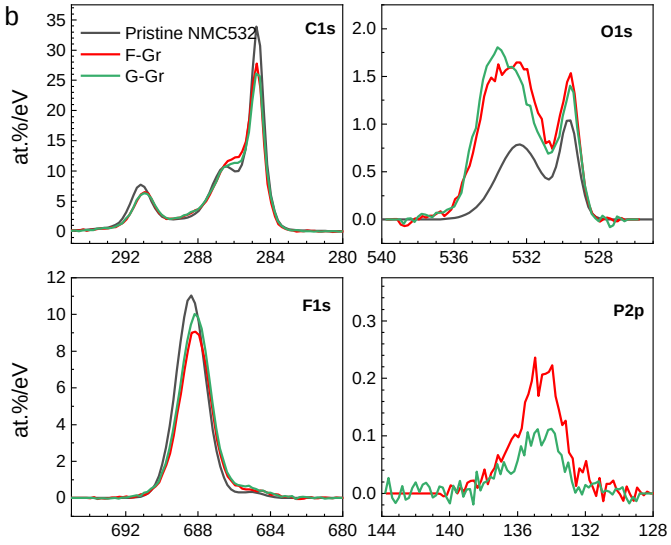
b
Pristine NMC532
F-Gr
G-Gr
C1s
O1s
F1s
P2p
at.%/eV

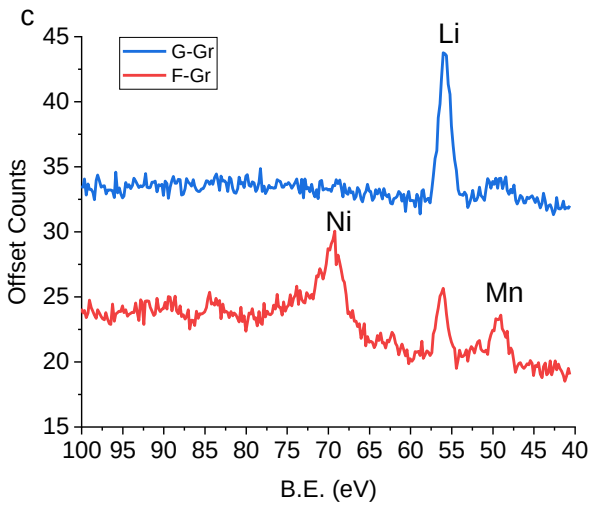

Figure 6. XPS results from the cells after cycling, including C1s, O1s, F1s, P2p for anodes (a) and cathodes (b) after cycling, as well as smaller binding energies for anodes (c).

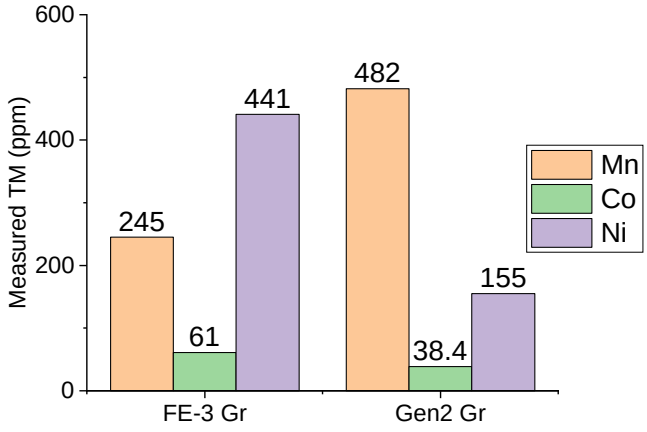

Figure 7. Transition metal content of the anodes after cycling for cells with preformed anodes.

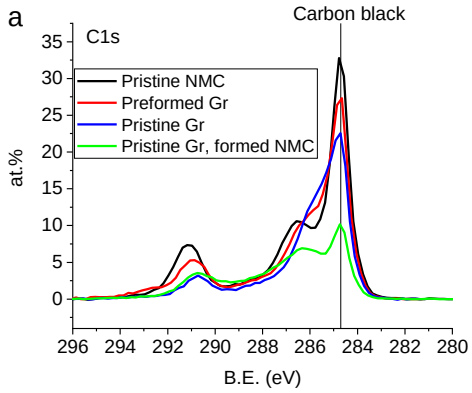
a
C1s
Carbon black
Pristine NMC
Preformed Gr
Pristine Gr
Pristine Gr, formed NMC
at.%
B.E. (eV)

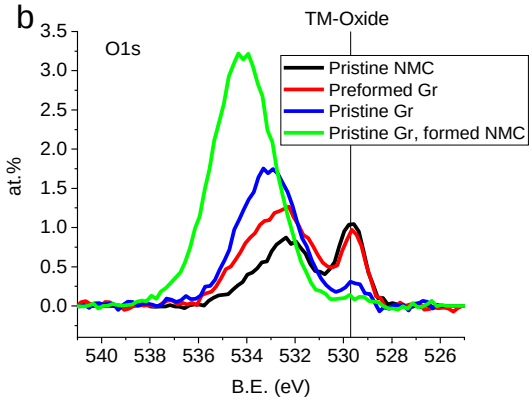
b
O1s
TM-Oxide
Pristine NMC
Preformed Gr
Pristine Gr
Pristine Gr, formed NMC
at.%
B.E. (eV)

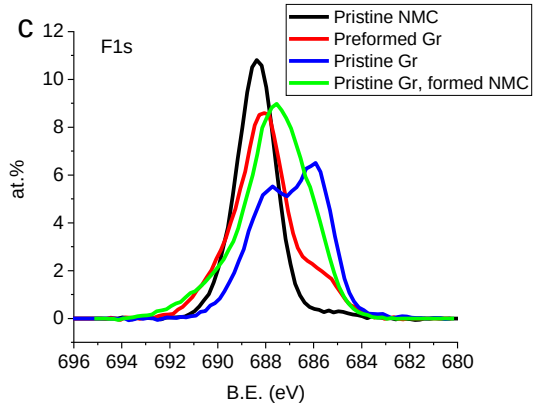
c
F1s
Pristine NMC
Preformed Gr
Pristine Gr
Pristine Gr, formed NMC
at.%
B.E. (eV)

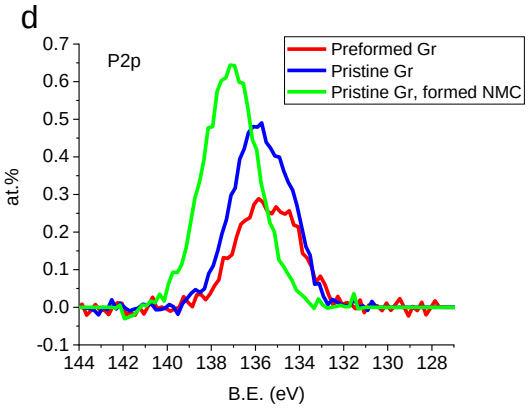
d
P2p
Preformed Gr
Pristine Gr
Pristine Gr, formed NMC
at.%
B.E. (eV)

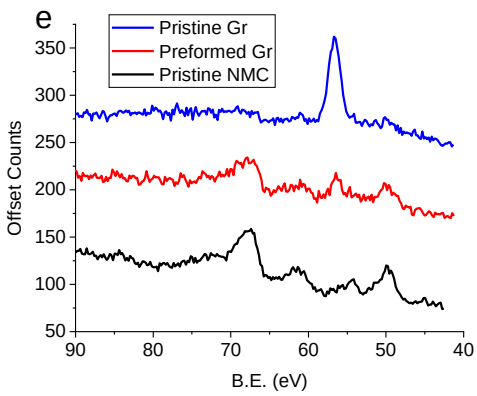
e
Pristine Gr
Preformed Gr
Pristine NMC
Offset Counts
B.E. (eV)

Figure 8. XPS results of the cathodes from cells formed with FE-3 electrolyte shown in Figure 3, showing C1s (a), O1s (b), F1s (c), P2p (d), and lower binding energies (e). For each plot, "Pristine NMC" denotes an uncycled cathode, "Preformed Gr" is a cathode cycled with F-Gr, "Pristine Gr" denotes a cathode cycled with a pristine graphite electrode with FE-3, and "Pristine Gr, formed NMC" denotes a cathode that had already been cycled with a pristine graphite electrode with FE-3, extracted, and reassembled with a new pristine graphite electrode, and cycled with FE-3.

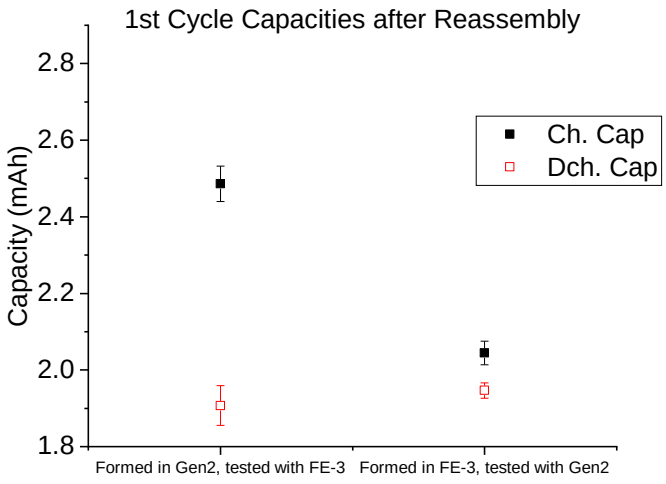

Figure 9. First charge and discharge capacities of cathode-anode pairs cycled with FE-3 after pretreatment with Gen2 (left) or cycled with Gen2 after pretreatment with FE-3 (right).